Neurotherapeutics (2021) 18:2692–2706
https://doi.org/10.1007/s13311-021-01126-2

ORIGINAL ARTICLE

Upregulation of AQP4 Improves Blood–Brain Barrier Integrity and Perihematomal Edema Following Intracerebral Hemorrhage

Hanwool Jeon[1,2] · Moinay Kim[1] · Wonhyoung Park[1,3] · Joon Seo Lim[4] · Eunyeup Lee[1,2] · Hyeuk Cha[1,2] · Jae Sung Ahn[1,3] · Jeong Hoon Kim[1,3] · Seok Ho Hong[1,3] · Ji Eun Park[3,5] · Eun-Jae Lee[2,3,6] · Chul-Woong Woo[7] · Seungjoo Lee[1,2,3]

Accepted: 7 September 2021 / Published online: 20 September 2021

Abstract

In intracerebral hemorrhage (ICH), delayed secondary neural damages largely occur from perihematomal edema (PHE) resulting from the disruption of the blood–brain barrier (BBB). PHE is often considered the principal cause of morbidity and mortality in patients with ICH. Nevertheless, the main cellular mechanism as well as the specific BBB component involved in the formation of PHE after ICH remains elusive. Herein, we evaluated the role of AQP4, a water channel expressed on the astrocytes of the BBB, in the formation of PHE in ICH. The static and dynamic functions of the BBB were evaluated by analyzing the microstructure and leakage assay. Protein changes in the PHE lesion were analyzed and the control mechanism of AQP4 expression by reactive oxygen species was also investigated. Delayed PHE formation due to BBB disruption after ICH was confirmed by the decreased coverage of multiple BBB components and increased dynamic leakages. Microstructure assay showed that among the BBB components, AQP4 showed a markedly decreased expression in the PHE lesions. The decrease in AQP4 was due to microenvironmental ROS derived from the hemorrhage and was restored by treatment with ROS scavenger. AQP4-deficient mice had significantly larger PHE lesions and unfavorable survival outcomes compared with wild-type mice. Our data identify AQP4 as a specific BBB-modulating target for alleviating PHE in ICH. Further comprehensive studies are needed to form the preclinical basis for the use of AQP4 enhancers as BBB modulators for preventing delayed cerebral edema after ICH.

Keywords Perihematomal edema · Vasogenic edema · Intracerebral hemorrhage · Vascular biology

Abbreviations

AQP4	Aquaporin-4
BV	Blood vessel
BBB	Blood-brain barrier
CaM	Calmodulin
DHE	Dihydroethidium
EED	Edema extension distance
ETbR	Endothelin B receptor
GFAP	Glial fibrillary acidic protein
H_2O_2	Hydrogen peroxide
ICH	Intracerebral hemorrhage

Hanwool Jeon, Moinay Kim, Wonhyoung Park, Joon Seo Lim, Jae Sung Ahn, Jeong Hoon Kim and Seok Ho Hong contributed equally to this work.

✉ Seungjoo Lee
changhill@gmail.com; rghree@amc.seoul.kr

[1] Department of Neurological Surgery, Asan Medical Center, University of Ulsan College of Medicine, Seoul, Republic of Korea

[2] Department of Medical Science, Asan Medical Center, Asan Medical Institute of Convergence Science and Technology, University of Ulsan College of Medicine, Seoul, Republic of Korea

[3] University of Ulsan College of Medicine, Seoul, Republic of Korea

[4] Clinical Research Center, Asan Medical Center, Asan Institute for Life Sciences, University of Ulsan College of Medicine, Seoul, Republic of Korea

[5] Department of Neuroradiology, Asan Medical Center, University of Ulsan College of Medicine, Seoul, Republic of Korea

[6] Department of Neurology, Asan Medical Center, University of Ulsan College of Medicine, Seoul, Republic of Korea

[7] Convergence Medicine Research Center, Asan Medical Center, Asan Institute for Life Sciences, University of Ulsan College of Medicine, Seoul, Republic of Korea

MR	Magnetic resonance
NAC	N-Acetylcysteine
PDGFR-beta	Platelet-derived growth factor receptor beta
PHE	Perihematomal edema
PKA	Protein kinase A
ROS	Reactive oxygen species
rPHE	Relative perihematomal edema

Introduction

Increases in BBB permeability in delayed cerebral edema after an intracerebral hemorrhage lead to significant morbidity and exacerbate clinical outcomes [1–3]. Nevertheless, the mechanism of the delayed increase in BBB permeability is mostly unknown, and the specific component of the BBB microenvironment involved in the formation of cerebral edema in intracerebral hemorrhage is yet to be identified [4]. Due to the cessation of blood supply, the movement of fluids after cerebral infarction is largely driven without energy support. As a result, the progressive changes in osmotic and hydrostatic conductivity of abnormal capillaries could be categorized into three phases: formation of ionic edema due to Na^+-K^+ channel failure, formation of vasogenic edema due to ischemia-induced capillary failure, and catastrophic failure with hemorrhagic transformation. Cytotoxic edema, or cellular swelling, manifests minutes after acute injuries to the central nervous system (CNS). Ionic edema, which refers to extracellular edema occurring in the presence of intact blood–brain barrier (BBB), forms immediately following cytotoxic edema. Vasogenic edema, which is extracellular edema that includes the extravasation of plasma proteins, manifests hours after the initial insult [3, 4].

The BBB permeability is canonically regulated by alterations in endothelial tight junctions and PDGFR-beta-controlled pericyte coverage [5, 6]; however, it is unclear whether these mechanisms also play a major role in the formation of PHE.

To date, 13 members of the AQP family have been discovered [7, 8], among which AQP4 is specifically localized at astrocyte surfaces of the blood–brain and cerebrospinal fluid-brain barriers [9]. AQPs are historically known to be passive transporters of water. However, the accumulated evidence in the last decade has highlighted the diverse function of AQPs beyond water homeostasis. For example, emerging biophysical evidence suggests that AQPs may also facilitate gas (CO_2) and cation transport. In addition, AQPs may be involved in the cell signaling for volume regulation and controlling the subcellular localization of other proteins by forming macromolecular complexes. Moreover, a subgroup of AQP water channels also facilitates transmembrane diffusion of small, polar solutes, water, and aquaglyceroporin [8, 10–12]. AQP1 is expressed in the apical membrane of choroid plexus epithelium and showed a protective role in hypertensive rats [13]. Conversely, AQP11 is expressed on brain endothelial cells and induces PHE, an effect associated with miR-27a-3p [14]. Importantly, AQP4 acts as a Janus-like water channel in cerebral edema formation [15], as it allows bidirectional flux of water through the cell membranes and facilitates water transport to and from the brain parenchyma [16]. Accordingly, both genetic deletion and overexpression of AQP4 have been shown to increase water accumulation in the brain after cerebral infarction and hemorrhage [17–19]. They are suggesting that the disease-specific microenvironment regulates the net function of AQP4 in cerebral edema. Thus, a targeted study is needed to identify the regulators of AQP4 expression in pathological conditions and determine if targeting the AQP4 regulator may confer clinical benefits in intracerebral hemorrhage. Edema is a hallmark of secondary CNS injuries after ischemic stroke or hemorrhage, and it is mainly mediated by AQP4. Targeting the subcellular localization of AQP4 in ischemia and hypoxia not only alleviates edema but also stabilizes the BBB or BSCB, thus leading to improved functional outcomes as shown in studies with CaM or PKA inhibition. Moreover, a recent study showed that targeting AQP4 reduces cerebral edema during the early post-stroke phase in mice. Although the above studies convincingly demonstrated the role of AQP4 in the early phase of cytotoxic edema, the role of AQP4 in vasogenic edema is still elusive. Therefore, we focused on the role of AQP4 in the delayed PHE formation by vasogenic edema after intracerebral hemorrhage [20, 21]. Herein, we investigated the significance of AQP4 in intracerebral hemorrhage as well as the therapeutic role of ROS scavenger as a microenvironmental modulator of AQP4 using animal models.

Methods

Animal Experiments

All animal experiments in this study were conducted under the approval and guideline of the Institutional Animal Care and Use Committee (IACUC) of Asan Institute for Life Sciences in Asan Medical Center. C57BL/6 mice (OrientBio, Seongnam-si, Gyeonggi-do, Republic of Korea) and aquaporin-4 knock-out ($AQP4^{-/-}$) mice (RIKEN, Saitama, Japan) at 7–10 weeks of age were used for experiments. To generate an intracerebral hemorrhage murine model, 50 µl of autologous blood collected from the retroorbital venous plexus was infused into the basal ganglia (coordinates: 2.0 mm (right), 0.2 mm (anterior), 3.7 mm (depth) apart from bregma) under general anesthesia with an intraperitoneal injection of ketamine (100 mg/kg) and xylazine hydrochloride (10 mg/kg); the infusion rate was continuously controlled

at a rate of 1.25 µl/min by an automated infusion system (Hamilton, Boston, MA, USA) [22]. T2-weighted magnetic resonance images (Bruker Pharmascan 9.0 T/160 mm, Ettlingen, Germany) were acquired on days 1, 3, and 7 after intracerebral hemorrhage induction. The parameters of MRI were as follows: repetition time = 4500.00 ms, echo time = 50.00 ms, averages = 2, echo spacing = 16.667 ms, matrix size = 256*256, slice thickness = 0.5 mm. The sizes of the hematoma and PHE were measured using the ImageJ software (NIH, Bethesda, MD, USA) and calculated using the equation shown below [23]: Since EED (edema extension distance) is not affected by hematoma size and reflects PHE change well, the PHE change was analyzed using EED. Therefore, the EED was calculated as follows [24, 25].

$$\text{EED (Edema extension distance)} = \sqrt[3]{\frac{\text{Edema volume} + \text{Hemorrhage volume}}{4/3\ X\pi}} - \sqrt[3]{\frac{\text{Hemorrhage volume}}{4/3\ X\pi}}$$

ROS scavenger (N-acetylcysteine [26], Catalog No: A7250, 200 mg/kg; Sigma), 6-hydroxy-2,5,7,8-tetramethylchroman-2-carboxylic acid (Trolox [27], Catalog No: 238813, 100 mg/kg; Sigma), functionally AQP4-enhancing substance (BQ-788 sodium salt [28], Catalog No: 1500, 3 mg/kg; Tocris Bioscience), and aquaporin inhibitor (2-nicotinamide-1,3,4-thiadiazole (TGN-020 [29], Catalog No: SML0136, 100 mg/kg; Sigma) were administered every other day for 14 days via intraperitoneal injection.

Immunofluorescence Staining and Histologic Analysis

The microstructures and dynamic leakages of BBB in PHE were investigated after intracerebral hemorrhage induction. The vascular structures were visualized by CD31 staining and lectin perfusion (DyLight-649 labeled lectin, Catalog No: DL-1178–1, 0.1 mg/mouse, Vector Laboratories). To assess the BBB leakage, Evans blue (Sigma, Catalog No: E2129, 2% in PBS) and dextran 10 kDa (Invitrogen, Catalog No: D1817) were each perfused for 12 h and 5 min prior to sacrifice. The brain tissue was fixed in two steps: perfusion with 4% paraformaldehyde for 5 min via the trans-cardiac route for pre-harvest fixation, and immersion in 4% paraformaldehyde for 24 h for post-harvest fixation. The fixed samples were serially dehydrated in 10 to 30% sucrose solutions for 24 h at each concentration. The fully prepared samples were sliced at a thickness of 60 µm followed by permeabilization with 0.3% Triton X-100 in phosphate-buffered saline solution for 10 min. To prevent non-specific antibody binding, the samples were blocked using 1% bovine serum albumin for 30 min. The samples were then treated with primary antibodies against the BBB components and incubated overnight in a cooling chamber. The primary antibodies used are as follows: CD13 and PDGFR-beta for pericytes; laminin for basement membrane; GFAP and S100-beta for activated astrocytes; aquaporin-4; and CD31 for endothelial cells. Fluorescence-tagged secondary antibodies were selected according to the species of the primary antibodies. DAPI was used for nuclear staining. The fluorescence images were acquired using LSCM 710 (Zeiss) and processed with the ZEN image software (Zeiss). For detection of specific proteins, the following antibodies and reagents were used: CD31 (BD Biosciences, Catalog No: 550274, 1:100; Merck, Catalog No: MAB1398Z; 1:100), PDGFR-beta (ebioscience, Catalog No: 14–1402-82, 1:100), GFAP (NOVUS, Catalog No:NB300-141,1:1000), AQP4(SANTACRUZ, Catalog No:SC-32739, 1:100 and allomone labs, Catalog No:AQP-004, 1:100), VE-cadherin (BD biosciences, Catalog No: 555289, 1:100), Claudin-5 (Invitrogen, Catalog No:35–2500, 1:200), Laminin (Sigma-Aldrich, Catalog No:L9393, 1:250), Ter119 (ebioscience, Catalog No: 14–5921-82, 1:100), and fluorescent conjugated secondary antibody (Bethyl, Donkey anti-goat FITC Catalog No: A50-101F; Donkey anti-goat Dylight 550, Catalog No:A50-101D3; Donkey anti-mouse FITC, Catalog No: A90-137F; Donkey anti-mouse Dylight 550, Catalog No: A90-137D3; Donkey anti-rabbit FITC, Catalog No: A120-108F; Donkey anti-rabbit Dylight 550, Catalog No: A120-108D3; biolegend, Goat anti-hamster Alexa 488, Catalog No: 405503; Goat anti-hamster Dylight 594, Catalog No: 405504; all secondary antibody dilutions: 1:500). The parameters of laser scanning confocal microscopy and numerical aperture of the utilized lens are as follows.

Objective lens	×20/0.80 M27
	×63/1.2 W
Dimensions	1024 × 1024
Pinhole	88 µm
Laser power	405 nm: 3.5%
	488 nm: 35%
	561 nm: 45%
	633 nm: 50%
Filters	Ch1: 410–480
	ChS1: 495–553
	ChS2: 563–650
	Ch2: 660–719
Refractory index	1.46

Three-Dimensional Blood Vessel Analysis

Three-dimensional images around the hematoma and edema were obtained instead of two-dimensional images to minimize the artifacts in measuring the BBB leakage. Before sacrifice, the mice were perfused with 488-lectin via the transcardiac route for 5 min and fixed according to the protocol mentioned earlier. The harvested samples were sliced at a thickness of 3 mm to fully include the lesion sites, followed by tissue clearing with the Binaree Tissue Clearing™ Kit (Binaree, Catalog No: HRTC-001) for 24 h in a warm bath. After the clearing process, the samples became transparent enough for the lasers to pass through. The transparent samples were adjusted to a refractive index of 1.45 by immersion in a mounting solution for 24 h. After embedding in low gelling temperature agarose (Sigma, Catalog No: A9414, 1% in distilled water), three-dimensional images were obtained using light-sheet microscopy (Z.1, Zeiss) with the following acquisition parameters: magnification = × 5/0.16, exposure time = 99.9 ms, zoom factor = 0.7. The acquired images were processed using ZEN image software (Zeiss).

In Vitro Experiments

Human astrocytes (Sciencell, Catalog No: 1800) and human brain endothelial cells (HBEC-5i, ATCC) were co-cultured in an in vitro system to recapitulate the astrocyte coverage around the vessels. Before co-culture, the astrocytes and endothelial cells were each incubated in astrocyte media (Sciencell, Catalog No: 1801) and endothelial cell growth media (Promocell, Catalog No: C-22010). The top surface of the polyester membrane (Corning) was coated with poly-L-lysine (Sigma, Catalog No: P6282) for 2 h. The bottom surface was coated with 0.1% gelatin in cell culture water (Sigma, Catalog No: G1393) for 2 h. Astrocytes and endothelial cells were seeded and stabilized sequentially for 2 h and then incubated for 48 h [30]. In the ROS treatment experiment, 50 µM and 100 µM of hydrogen peroxide (H_2O_2) (MPbio, Catalog No: 7722–84-1) were added to the co-culture media; then, 100 µM of the ROS scavenger N-acetylcysteine (Sigma, Catalog No: A7250) was treated for 4 h and replaced once every hour. Then, the co-cultured astrocytes and endothelial cells were washed and fixed with 4% cold paraformaldehyde and collected for Western blot and immunofluorescence analysis.

Protein Analysis

The PHE region in mice was microdissected and lysed in 0.5% PBS-T (Triton X-100) solution. According to the manufacturer's protocol, protein levels were quantified using the cytokine protein array kit (RayBiotech C2000, Catalog No: AAM-CYT-2000). Human astrocytes were lysed in RIPA lysis buffer (ENZO Life sciences, Catalog No: ADI-80–1284) containing phosphatase inhibitor cocktail (Sigma, Catalog No: P5726 and P0044) and proteinase inhibitor cocktail (Roche, Catalog No: 11697498001). The cell lysates' protein concentration was determined by bicinchoninic acid assay (Thermo Fisher Scientific, Catalog No: 23227), and the cell lysates were then resolved in SDS-PAGE gels. For detection of specific proteins, the following antibodies were used: AQP4 (allomone labs, Catalog No: AQP-004, 1:1000), Beta-actin (SANTA CRUZ, Catalog No: sc-47778, 1:1000), total Akt (Cell signaling, Catalog No:9272, 1:1000), p-Akt (Cell signaling, Catalog No: 9271, 1:1000), total FoxO3a (Cell signaling, Catalog No: 2497, 1:1000), p-FoxO3a (Cell signaling, Catalog No: 9466, 1:1000), p-Erk (Cell signaling, Catalog No: 4376, 1:1000), and total Erk (Cell signaling, Catalog No: 9102, 1:1000). Western blotting analysis was performed according to standard procedures, and the protein signals were developed by the enhanced Amersham ECL western blotting analysis system (GE Healthcare, Catalog No: RPN2232).

Reactive Oxygen Species Analysis

After ICH, PHE areas of the brain specimens were obtained after MRI and used collagenase/Dispase enzyme (Roche, Catalog No: 10269638001) to digest tissues before single-cell isolation. After digestion, cells were passed through a 40-µm cell strainer, and myelin and cell debris were removed by 22% percoll (Sigma, Catalog No: P4937) gradient centrifugation. Single cells were resuspended in 2% FBS in PBS buffer and labeled with Cellrox-FITC (Invitrogen, Catalog No: C10444), and CD31-APC/Fire 750 (Biolegend, Catalog No: 102528, 1:500) antibodies. For intracellular staining, single cells were permeabilized and fixed with BD Cytofix/cytoperm Fixation/Permeabilization Kit (BD Biosciences, Catalog No: 554714) after surface staining. The cells were washed twice with 1 × perm/wash buffer and stained with NeuN-PE (NOVUS, Catalog No: NBP1-92693PE, 1:500), and GFAP-647 (BD biosciences, Catalog No: 561470, 1:500). Flow cytometry data were obtained from BD FACSCanto II workstation (BD Biosciences) and analyzed using FlowJo software.

Inclusion and Exclusion Criteria

Inclusion and exclusion criteria are addressed below.

Inclusion Criteria

1. C57/B6 male mice with age 8~10 weeks, female mice were excluded due to the effect of hormonal variations
2. Purchased from Orient Bio Co. and adapted in inbreed facility

3. Healthy without evidence of hypertension, anemia, vasculopathy, and neurological deficiency
4. Mice survived after intracerebral hemorrhage induction at immediate post-procedure period
5. Mice successfully weaned from anesthesia

Exclusion Criteria

1. Profound hemorrhage over expected intracerebral hemorrhage induction (secondary hemorrhage)
2. Mice with unexpected small intracerebral hemorrhage volume (model production failure)
3. Brain death or imminent death after procedure
4. Seizure requiring acute management
5. Post-cardiac arrest with suspected significant anoxic brain injury

Randomization and Blinding

After screening, eligible mice were randomly allocated to the control group or ROS scavenger group (N-acetylcysteine, BQ-788 each) in a 1:1 ratio using an interactive Web response system. Allocation will be by randomly permuted blocks and stratified by hemorrhage size to enhance balance. Partial blinding was applied in the present study. The agents were not blinded because it was not feasible to manufacture and manage pseudo-drugs. However, procedural blinding was achieved with separate experiments. The researcher made a model that was not involved in radiologic measurements and analyses. Each mouse was assigned a unique number and measurement values were integrated by an independent researcher.

Sample Size Calculation

The primary endpoint for the study is the composite of survival outcome and perihematomal edema size at 1 week after randomization. We calculated the sample size by assuming that the primary endpoint rate would be 30% in the ROS scavenger group and that the edema reduction with ROS scavenger would be 40%. With 80% power and a one-sided level of significance of 0.05, 14 mice were required per treatment group. The software PASS version 12 (NCSS, LLC; Kaysville, Utah, USA) was used for the sample size calculation.

Statistical Analysis

Values are reported as mean ± standard deviation unless indicated otherwise. For continuous data in animal studies, statistical significance was determined by the Mann–Whitney *U* test for comparison between two groups and the Kruskal–Wallis test with Bonferroni correction for comparison among multiple groups. The log-rank test was used for survival analysis. All statistical analyses were performed with PASW Statistics 18 (SPSS). Differences were considered to be statistically significant at $P < 0.05$.

Results

Phenotypic Analysis of the Murine Model of Intracerebral Hemorrhage

We generated a murine model of intracerebral hemorrhage by injecting 50 µl of autologous blood into the right basal ganglia, a region commonly affected by intracerebral hemorrhage (Fig. 1a). We investigated whether the model aptly recapitulates the PHE formation as observed in patients with intracerebral hemorrhage. We observed the chronological changes of PHE by T2-weighted MRI and found that the volume of PHE peaked at 3–4 days and resolved within 14 days (Fig. 1b); similarly, the hematoma also resolved within 14 days. To evaluate the vascular permeability in the PHE, we systemically perfused the mice with Evans blue dye, which does not leak into the cerebral tissues in physiological conditions because multiple BBB components tightly cover the cerebrovascular structure. In our murine model of intracerebral hemorrhage, the Evans blue dye had leaked significantly in the PHE region (Fig. 1c, d). Lectin perfusion assay also showed large amounts of leakage through the blood vessels, which showed characteristic dilation in the PHE region (Fig. 1e).

To detect the protein changes in PHE, we performed multifaceted analysis on micro-capture dissection of the PHE region by using protein array and confocal microscopy. Among the proteins associated with BBB, AQP4 showed a markedly reduced expression in the PHE region (Fig. 2a, c). Confocal microscopy also showed that the widespread expression of AQP4 on the blood vessels in the normal brain was notably reduced in PHE rather than other BBB components (Fig. 2b).

Genetically modified AQP4$^{-/-}$ mice showed a notably more rapid and widespread PHE formation as well as increased vascular leakage compared with wild-type mice (Fig. 2f). AQP4$^{-/-}$ mice also showed a significantly poorer survival following hemorrhage induction (Fig. 2d); moreover, whereas wild-type and AQP4$^{-/-}$ mice did not show a significant difference in the hematoma volume, the edema volume was significantly greater in AQP4$^{-/-}$ mice (Fig. 2e). These results were recapitulated in pharmacological experiments using TGN-020, an AQP4 inhibitor (Fig. 3a, b); compared with control mice without pharmacological treatment, mice treated with AQP4 inhibitors showed significantly delayed PHE resolution, increased PHE formation (Fig. 3d), increased vascular leakage (Fig. 3c, e), and reduced survival (Fig. 3f).

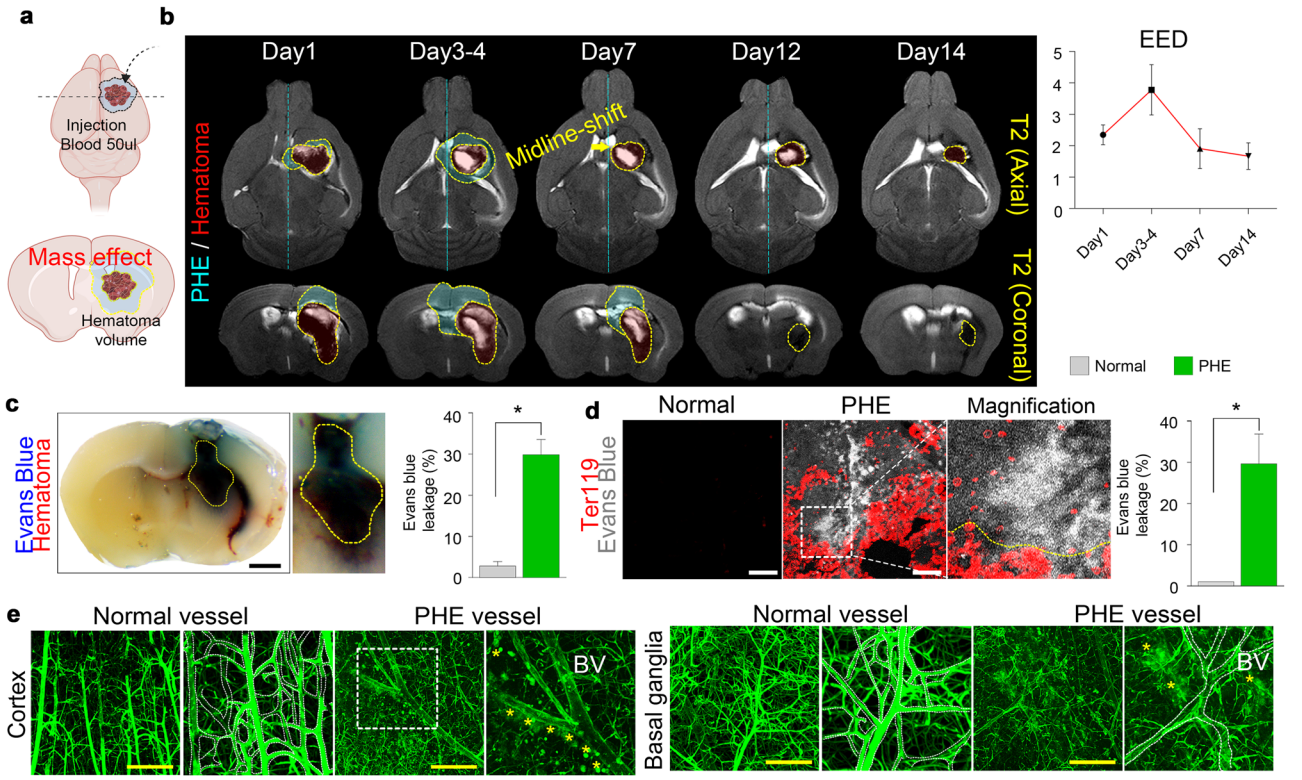

Fig. 1 AQP4 is downregulated in perihematomal edema, and genetic deletion of AQP4 exacerbates intracerebral hemorrhage in mice. **a** Illustration depicting the generation of the animal model of intracerebral hemorrhage. **b** MR images showing the chronological changes in perihematomal edema (PHE) and hematoma in the intracerebral hemorrhage animal model. **c** Representative gross image of coronal brain section showing Evans blue leakage. **d** Immunofluorescence staining of Ter119 + red blood cells and Evans blue leakage in the PHE area (magnification, × 20). **e** Lectin perfusion assay showing abnormal vasodilation and lectin leakage in the PHE (magnification, × 5); black scale bar, 100 μm; yellow scale bar, 200 μm. Data are mean ± SD. $^{*}P < 0.05$, $^{**}P < 0.01$

Hemorrhage-Derived Reactive Oxygen Species (ROS) Downregulates AQP4 Expression in Astrocytes

Our antibody-based protein array showed that AQP4 expression was significantly decreased in the PHE region, and we also observed that PHE was aggravated in AQP4$^{-/-}$ mice. These results suggest that some factors in PHE may reduce AQP4 expression. We thus tested whether hemorrhage-derived products (i.e., iron, urokinase, thrombin, and reactive oxygen species [ROS]) downregulate the AQP4 expression in vitro (Supplementary Fig. 1). We found that ROS generated by intracerebral hemorrhage significantly reduced the AQP4 expression in the PHE. Therefore, we performed a co-culture of astrocytes and endothelial cells to confirm the role of ROS in regulating AQP4 expression in astrocytes (Fig. 4a). AQP4 expression was significantly reduced upon treatment with H_2O_2, which was effectively negated by co-treatment with N-acetylcysteine (NAC), a potent ROS scavenger (Fig. 4b, c).

We also found that mice with intracerebral hemorrhage showed prominent activation of astrocytes (i.e., increased S100-beta expression, a higher number of dendrites) in their PHE region, which was also effectively negated upon co-treatment with NAC (Supplementary Fig. 2). In the PHE regions, the AQP4 expression reduction was accompanied by a significant elimination of astrocytes coverage on the blood vessels (Fig. 4d). Interestingly, the ROS expression site coincidently overlapped with the PHE region (Fig. 4e) and the region with reduced AQP4 expression. In this area, astrocyte coverages were eliminated from blood vessels. Still, they were effectively restored by ROS scavenger treatment (Fig. 4f), thus showing that ROS regulates AQP4 expression and astrocyte coverage on the blood vessels in the PHE. We then performed microdissection of the PHE region to identify the source of ROS production and found that the majority of ROS was produced by hemorrhage-derived products, astrocytes, and neurons (Supplementary Fig. 3). Our results collectively indicate that hemorrhage-derived ROS is a microenvironmental regulator of AQP4 expression and astrocyte coverage in PHE.

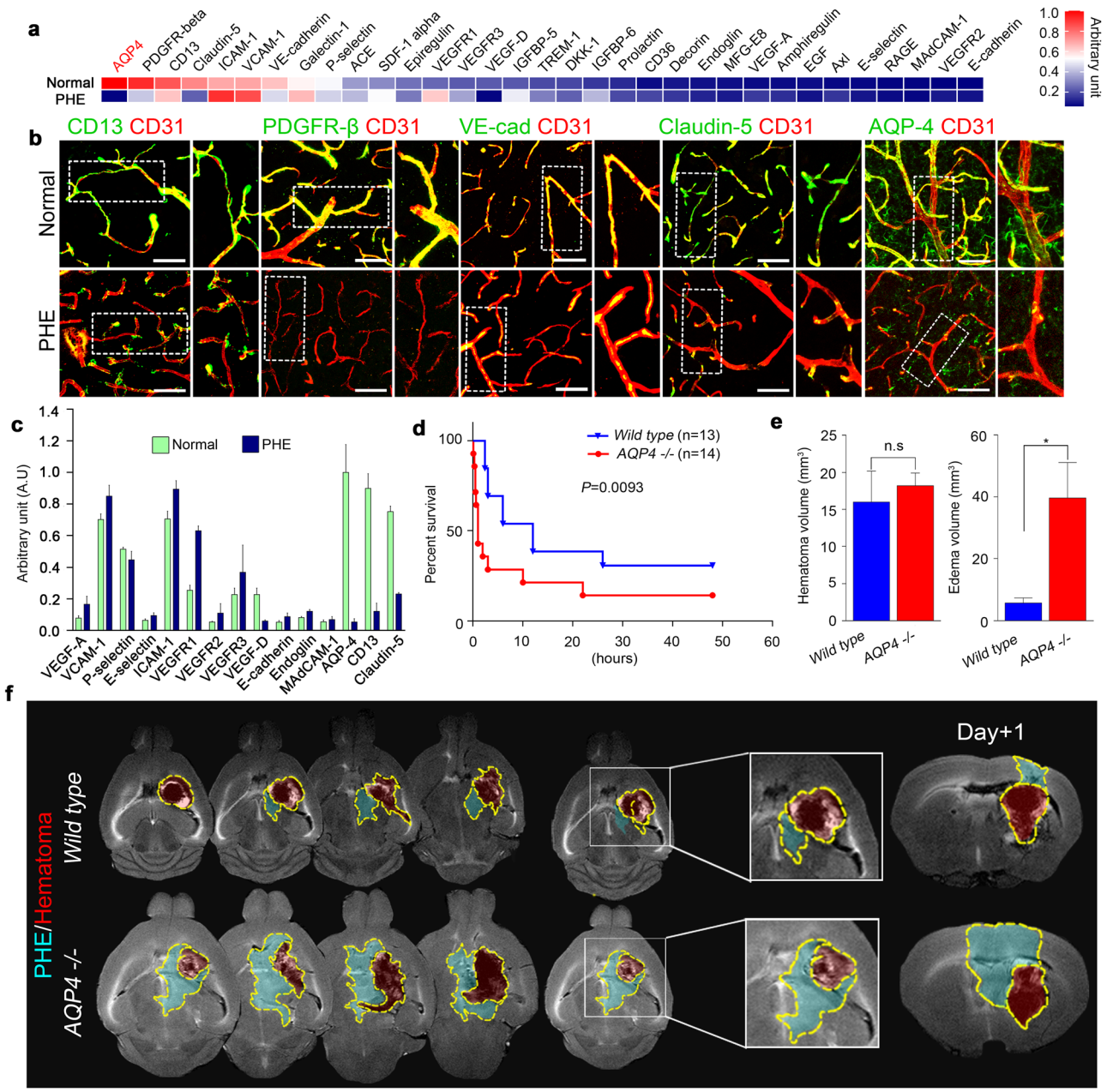

Fig. 2 Decreased AQP4 expression in PHE is associated with poor survival outcomes. **a** Protein array of tissues from normal and PHE sites. **b** Representative confocal microscopic images of vascular-associated molecules in normal and PHE tissues (magnification × 20). **c** Quantification of vascular-associated proteins in the PHE region. **d** Survival curves of wild-type and AQP4$^{-/-}$ mice after intracerebral hemorrhage. **e** Hematoma volumes and edema volumes of wild-type and AQP4$^{-/-}$ mice after intracerebral hemorrhage. **f** MR images showing the chronological changes of PHE and hematoma in wild-type and AQP4$^{-/-}$ mice. White scale bar, 50 μm. Data are mean ± SD. *$P < 0.05$. *Data in **a**, **b**, **c**, and **e** were obtained at post-ICH day 3

ROS Scavenger and AQP4 Enhancer Alleviate Perihematomal Edema by Improving Blood–Brain Barrier Integrity

We then investigated whether treatment with ROS scavengers, NAC, or Trolox can protect against the effects of intracerebral hemorrhage, reduce PHE, and restore the AQP4 expression. We also tested whether treatment with BQ-788, which enhances the AQP4 expression by antagonizing the endothelin B receptor (ETbR) [31], can also produce analogous effects with ROS scavengers. Each drug was administered every other day for 2 weeks after the hemorrhage induction (Fig. 5a). Both ROS scavengers and BQ-788 effectively inhibited PHE formation

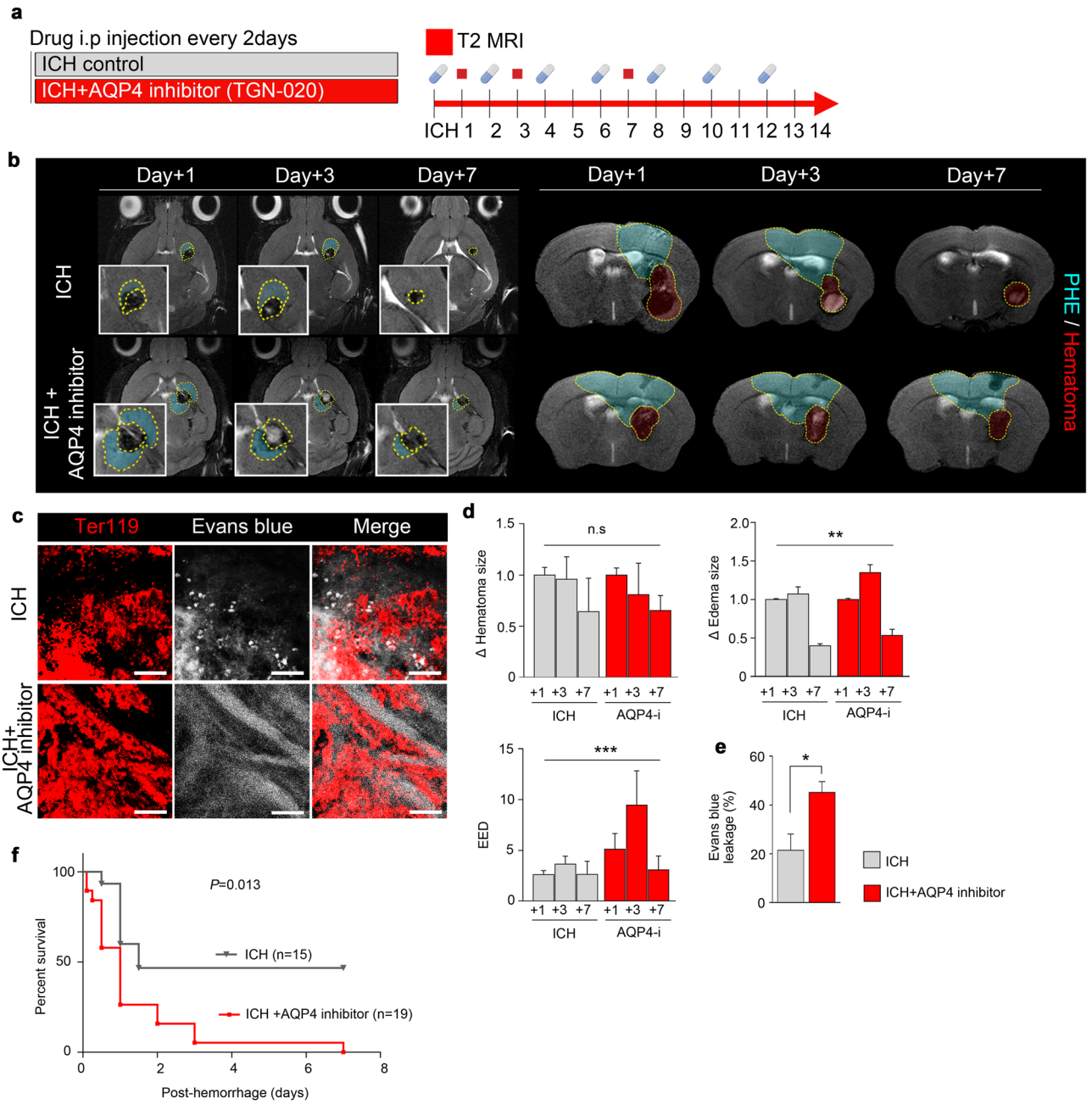

Fig. 3 Inhibition of AQP4 worsens survival outcomes by exacerbating PHE and slowing the resolution of intracerebral hemorrhage. **a** AQP4 inhibitor TGN-020 (100 mg/kg) was administered in animal models of intracerebral hemorrhage. **b** MR images taken at 1, 3, and 7 days after intracerebral hemorrhage in mice treated with or without AQP4 inhibitor. **c** Immunofluorescence staining of Ter119 + red blood cells and Evans blue leakage (magnification, × 20). **d**, **e** Quantification of the changes in the sizes of hematoma, edema, relative PHE in T2WI of MRI and Evans blue leakage in confocal microscopy of PHE. **f** Kaplan–Meier survival curves of mice treated with or without AQP4 inhibitor after intracerebral hemorrhage. Data are mean ± SD. $^{*}P < 0.05$, $^{**}P < 0.01$, $^{***}P < 0.001$

(Fig. 5b) and BBB leakage (Fig. 5c). Moreover, treatment with an ROS scavenger or an AQP enhancer resulted in improved survival rates (Fig. 5d). Similar to the result in AQP4$^{-/-}$ mice, ROS scavengers and AQP4 enhancer did not induce significant differences in the hematoma size (Fig. 5e) after hemorrhage induction but led to substantial reductions in the PHE extent (Fig. 5f) and EED corrected by the amount of hemorrhage (Fig. 5g). In addition, NAC treatment alleviated the PHE in AQP4-/- mice with cerebral hemorrhage (Supplementary Fig. 5a, c–e) and improved their survival rates (Supplementary Fig. 5b).

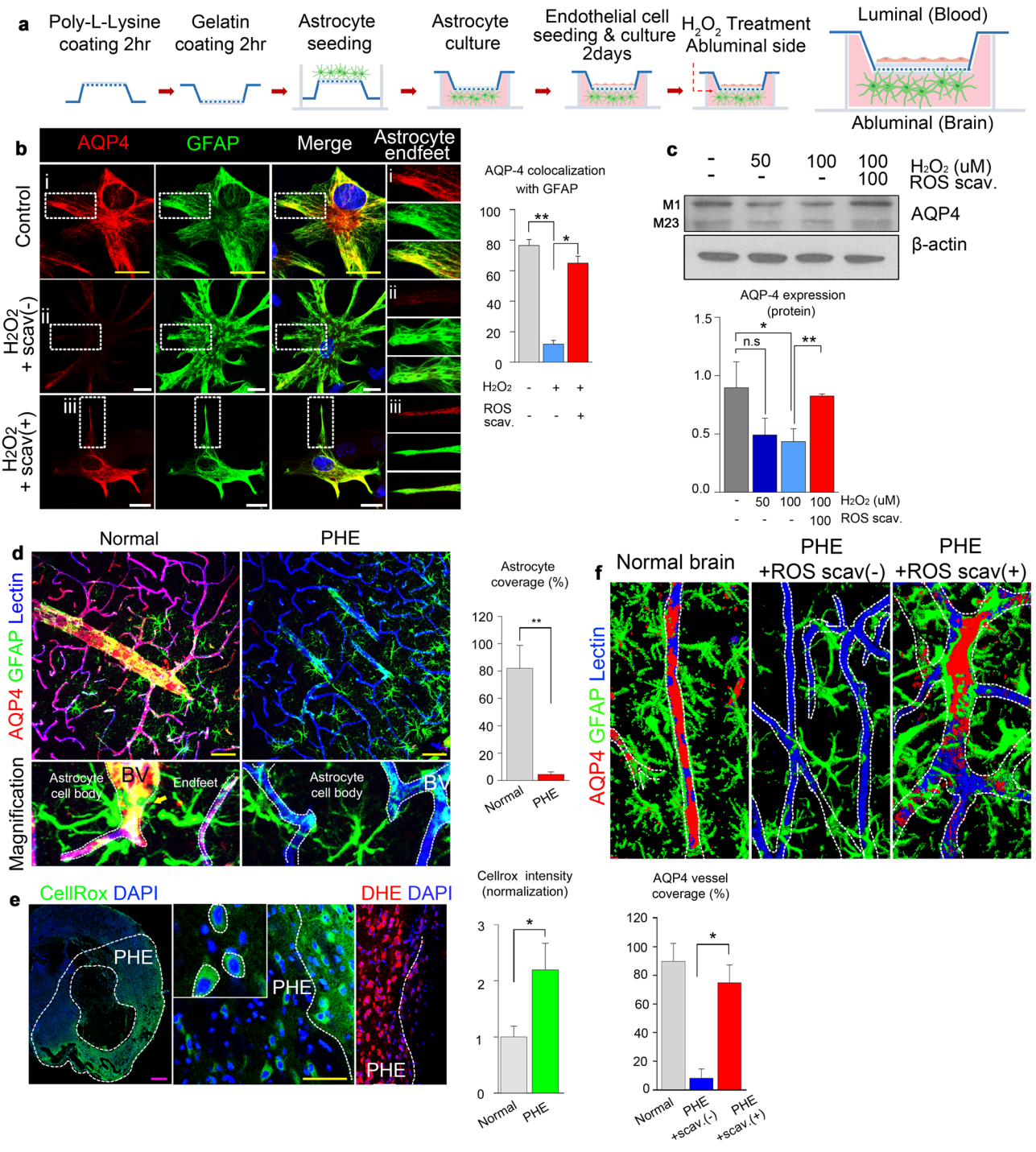

Fig. 4 Hemorrhage-derived reactive oxygen species regulate AQP4 expression in intracerebral hemorrhage. **a** Illustration of the in vitro co-culture system of astrocytes and endothelial cells. **b** Representative confocal images of AQP4 in the astrocyte end-feet under treatment with H_2O_2 with or without ROS scavenger (magnification, ×63). **c** Expression levels of AQP4 in astrocytes in the co-culture under treatment with H_2O_2 with or without ROS scavenger in indicated concentrations. **d** Representative confocal images showing AQP4 expression in the astrocyte-foot process in normal tissue and PHE tissue (magnification, ×20). **e** Representative confocal images showing ROS expression (CellRox, DHE) in the PHE area (magnification, ×20). **f** AQP4 expression in the PHE region with or without ROS scavenger treatment. White scale bar, 20 μm; yellow scale bar, 50 μm; magenta scale bar, 500 μm. Data are mean ± SD. *$P < 0.05$, **$P < 0.01$

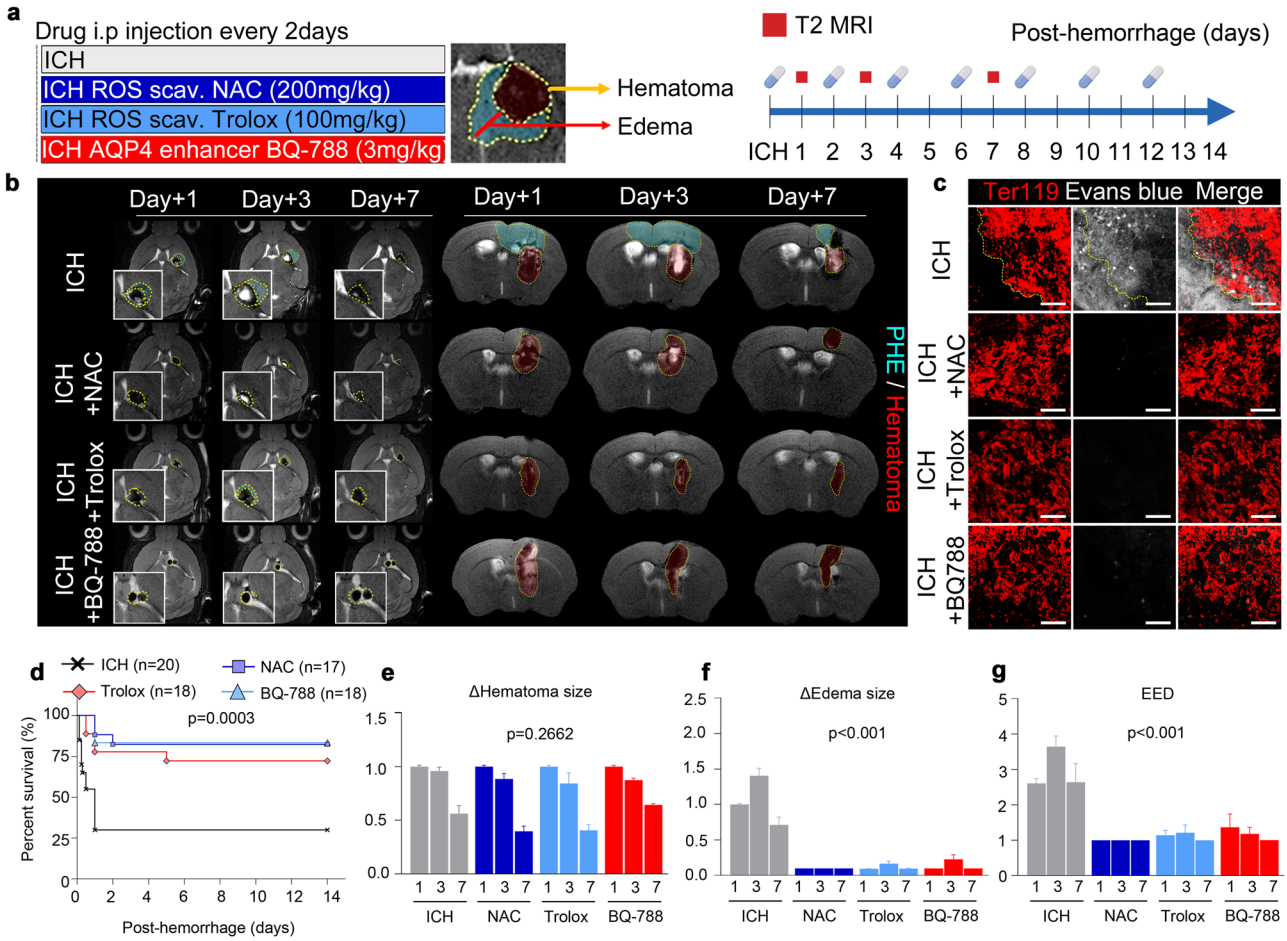

Fig. 5 ROS scavenger and AQP4 enhancer reduce perihematomal edema via improvement of blood–brain barrier integrity. **a** Dosing schedule of the ROS scavengers (NAC, Trolox) and the AQP4 enhancer (BQ-788) and the MRI schedule. **b** T2-weighted MRI images acquired at 1, 3, and 7 days after intracerebral hemorrhage showing the areas of PHE and hematoma. **c** Evans blue leakage assay demonstrating the improving leakages by ROS scavenger (NAC and Trolox) and AQP4 enhancer (BQ-788) (magnification, ×20). **d** Survival curves of the mice after intracerebral hemorrhage. **e**, **f**, **g** Changes in the sizes of hematoma, edema, and EED in the PHE region at 1, 3, and 7 days after intracerebral hemorrhage in mice. Scale bar, 50 μm. Data are mean ± SD

The changes in the BBB components were examined to reveal the cellular mechanism of PHE prevention by ROS scavenger and AQP4 enhancer. Both the ROS scavenger and the AQP4 enhancer significantly restored the expression levels of PDGFR-beta (Fig. 6a), VE-cadherin (Fig. 6b), and laminin (Fig. 6d), AQP4 (Fig. 6c), and astrocyte coverage (Fig. 6f). Notably, the ROS scavenger and the AQP4 enhancer showed comparable beneficial effects on the BBB microstructures. The expression of tight junction protein Claudin-5 was also increased upon treatment with an ROS scavenger or an AQP4 enhancer (Fig. 6e). These results collectively indicate that ROS is responsible for the pathophysiology of the PHE formation through the BBB disruption due to reduced AQP4 expression in astrocytes. AQP4 enhancement is effective in restoring the BBB's structural integrity. Figure 6g illustrates our findings on the structural changes in the BBB following intracerebral hemorrhage.

Discussion

Most patients with intracerebral hemorrhage develop varying degrees of PHE, which adversely affects the clinical course by increasing intracranial pressure [4, 32, 33]. For this reason, the resolution of PHE is vital for reducing morbidity and mortality. However, there are no direct treatments for PHE. The indirect treatment of removing the excessive accumulation of water from the brain parenchyma by inducing osmotic diuresis has shown unsatisfactory results [1]. Therefore, our results on the use of ROS scavenger and AQP4 enhancer to reduce the PHE volume in patients with intracerebral hemorrhage seem promising.

Early PHE is mainly caused by the Na^+-K^+ pump dysfunction, which is due to insufficient oxygen and energy supply by the microvascular shutdown in intracerebral hemorrhage [33]. The resulting disruption of the ion gradient

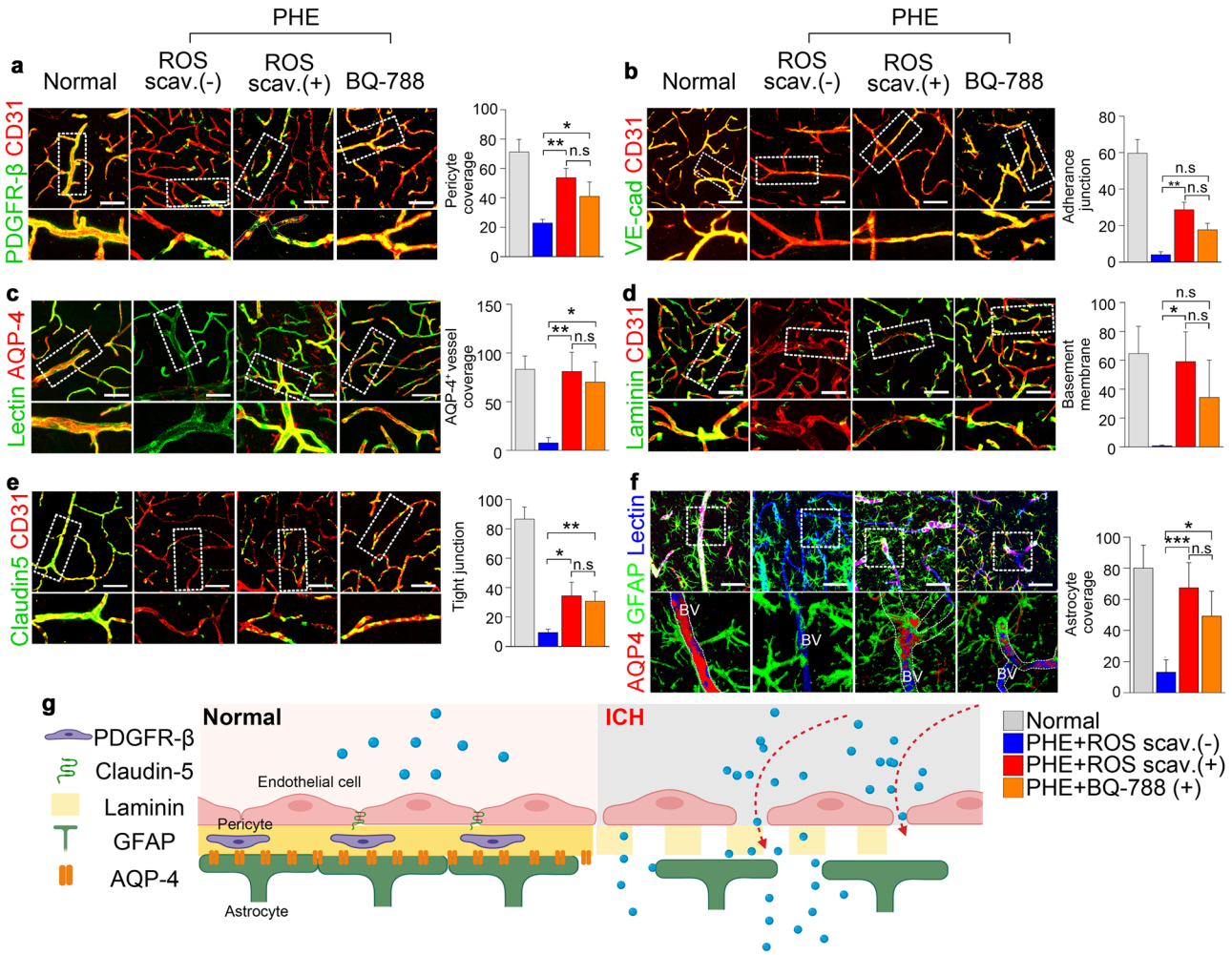

Fig. 6 Analysis of multiple components of the BBB in intracerebral hemorrhage. **a**, **b**, **c**, **d**, **e**, **f** Confocal microscopy of the BBB microstructures in the normal area and PHE area under the indicated conditions. Pericyte, adherence and tight junction, and basement membrane integrity were slightly disrupted in PHE region, but rescued by ROS scavenger and AQP 4 stabilizer. AQP 4 expression was prominently decreased in PHE and rescued by ROS scavenger and AQP 4 stabilizer (magnification, × 20). **g** Illustration showing the microstructure of the BBB under condition and after intracerebral hemorrhage. In the steady state, the BBB is a structurally stable complex formed by the pericyte (PDGFR-beta), tight junction (claudin-5), basement membrane (laminin), and end-feet of the astrocyte process. However, after intracerebral hemorrhage, PHE occurs due to the disruption of the BBB structure. Among the BBB structures of microvessels, pericyte, laminin, VE-cadherin, and astrocyte coverage are decreased in PHE. Scale bar, 50 μm. Data are mean ± SD. $*P < 0.05$, $**P < 0.01$, $***P < 0.001$. *ROS scav. (+): ROS scavenger treatment

between cell membranes leads to cytotoxic edema in the brain parenchyma. The brain is a highly active and plastic organ with significant energetic needs, and intracerebral hemorrhage could lead to disturbances in the energetic balance or glia-neuron metabolic interaction. Under physiological conditions, the major energy source for the brain is glucose [34]. Although neurons require a high amount of energy, they possess a minimal energy reserve that can satisfy only a small portion of the energy demand. Therefore, neurons are dependent on the supply of energy substrates such as lactate from the blood through the blood–brain barrier (BBB) and astrocytes (i.e., astrocyte-neuron lactate shuttle [ANLS]). BBB and astrocytes that are damaged under the PHE condition cannot properly supply energy substrates to neurons, leading to the aggravation of neuronal death-associated edema [35–40].

Conversely, as shown in our animal model of intracerebral hemorrhage, delayed PHE can occur due to excessive water leakage through the disrupted BBB or defects in removing excessive water through water channels [41]. In clinical practice, delayed PHE resulting from disruption of the BBB is often more problematic than cytotoxic edema that occurs immediately after hemorrhage [42]. The BBB disruption in PHE is due to inflammatory response, excitotoxicity, and increased free radicals; particularly, the increases in interleukin-1, 2, and 6 [43] as well as activated MMP-3, 9

cascade [44] in astrocytes by hemorrhage-induced inflammation result in tight junction damage [45]. As a result, toxic substances such as inflammatory cells [46], urokinase [47], thrombin [48], and haptoglobin [49] in the bloodstream can leak through the disrupted BBB and potentiate delayed PHE along with additional local inflammation. Subsequent inflammatory reactions that occur in the PHE activate the MMP cascade and increase the production of reactive oxygen–nitrogen species ($^{\bullet}$O2-, H_2O_2, $^{\bullet}$OH-, $^{\bullet}$NO, ONOO-) [50] and glutamate from glial cells such as activated microglia and astrocytes [51].

In our current study, the AQP4 expression on BBB's astrocyte coverage was reduced by ROS generated in intracerebral hemorrhage. Because the astrocyte coverage functions as the outer skeleton in maintaining overall BBB integrity, the decrease of AQP4 expression on astrocytes resulted in disrupting the BBB microstructures, including pericyte, basement membrane, and astrocyte coverage. As a result, leakage through BBB occurred rapidly, and PHE developed in the early stage of intracerebral hemorrhage.

In eukaryotic cells, ROS are generally produced in the reactions catalyzed by NAD(P)H oxidase and other specialized oxidases as well as the by-product of redox reactions. Intracellular ROS synthesis is regulated by various hormones, cytokines, and growth factors; however, in intracerebral hemorrhage, a large amount of extracellular ROS is generated from hemoglobin and ferrous end products [52, 53]. An increase in the ROS levels above a certain threshold is accompanied by detrimental processes for cell survival, such as lipid peroxidation and oxidative modification of proteins and nucleic acids. In our additional experiment, we found that ROS generated in intracerebral hemorrhage did not significantly alter the expression levels of cell signaling molecules involved in the survival and proliferation of astrocytes such as Erk, Akt, and FOXO3a (Supplementary Fig. 4). Thus, ROS is not likely to have affected the expression of AQP4 through the proliferative signaling pathway in astrocytes. However, some studies have shown that hypothermia, calcium receptor, and calmodulin-mediated mechanisms affect the surface trafficking of AQP4. In addition, ROS may also affect the expression level of AQP4 or its surface localization [54, 55]. Considering our in vitro experiments about the ROS-mediated AQP4 expression reduction in astrocytes, ROS seems to decrease the AQP4 expression through cellular mechanisms other than the canonical proliferative signaling cascade or post-translational modification.

The current treatment modalities for PHE are mostly indirect methods in which the excess water in the brain parenchyma is removed by administering hyper-osmotic agents such as mannitol and hypertonic saline [2]. However, the indirect methods have limited effects and often entail adverse effects such as rebound edema and renal toxicity. There are some direct strategies for alleviating PHE, which involve increasing the expression or function of the defective components of the BBB. A representative direct method is the administration of HMG-CoA reductase (e.g., atorvastatin). They showed pleiotropic effects in the tandem proliferation of pericytes, thereby improving the BBB's pericyte coverage, followed by reducing PHE's degree [56–58]. However, such direct methods seem to be primarily effective in preventing PHE development in patients taking the drug prior to the intracerebral hemorrhage, rather than alleviating the PHE after it has formed. Other direct methods include glibenclamide, which suppresses the functions of MMP-9 that are increased in intracerebral hemorrhage and induces local inflammation. Still, glibenclamide effects are yet to be fully supported through clinical trials [59]. In this aspect, our study is notable in that it focused on astrocytes, which are relatively overlooked but comprise the largest proportion of cells in the brain. Specifically, we sought to improve the BBB coverage by astrocytes in alleviating PHE. We also found that enhancing the expression and function of AQP4 in astrocytes is an effective way to achieve this goal. AQP4 in the end-feet of astrocytes is advantageous as a clinical target because it maintains the BBB's structural integrity to suppress the development of the PHE and can actively clear existing PHE. Considering that there are no clinically proven methods for directly alleviating PHE, our results on the potential therapeutic effect of AQP4 modulation seem promising.

AQPs have been validated as an important drug target, but no single drug has been approved to successfully target them. Although some potential AQP modulators have been identified, there are still challenges associated with developing better modulators such as the druggability of the target and the suitability of the assay methods used for identifying the modulators. Since AQP4 is also still an elusive drug target, it may be better to consider alternative routes to the traditional pore-blocking approach such as gene transfer or targeting the membrane localization of AQP4 [60, 61]. In mice treated with TGN-020, the expression of AQP4 was lower than that in untreated control mice, followed by more prominent PHE formation and poorer survival outcomes. However, the AQP4 inhibition experiment is limited in that the reversible effect of AQP4 targeting could not be assessed. Therefore, the cell surface expression of AQP4 should be evaluated through in vitro experiments to assess the reversibility according to the tonicity of targeting agents [20, 62].

In this study, TGN-020 was found to inhibit AQP4 based on *Xenopus laevis* oocyte swelling assays. However, there are concerns that the inhibitory action of TGN-020 is not readily reproducible in other assays, and that TGN-020 has effects on brain water transport independent of AQP4, thus confounding the interpretation of in vivo studies. In addition, the off-target effects of TGN-020 are largely unknown. Accordingly, the degree of increase in the edema volume in

mice treated with TGN-020 was far smaller than that shown in AQP4$^{-/-}$ mice, which likely reflects the suboptimal inhibitory capacity of TGN-020 against AQP4. Therefore, the action of TGN-020 on AQP4 is somewhat ambiguous and requires careful interpretation. Although the mechanism of the inhibition of AQP4 by TGN-020 could not be elucidated in the current study, our results have clearly demonstrated the in vivo inhibitory role of TGN-020 on AQP4 as the PHE of mice treated with TGN-020 was significantly more severe than that in control mice. The mode and mechanism of AQP4 inhibition by TGN-020 should be further identified in future studies [63].

Treatment with ROS scavengers restored the expression of AQP4 in vivo and in vitro and improved the BBB's overall integrity; notably, treatment with AQP4 enhancer produced similar beneficial effects, indicating the potential usefulness of AQP4 as a clinical target in ROS-mediated neurological diseases. The ROS scavenger has been known to reduce the edema by modulating local inflammation; however, our results collectively indicate that the ROS scavenger could reduce the PHE by restoring the AQP4 expression and subsequently improving the BBB integrity. Our culture system is a 2D culture system using a Transwell. Therefore, there might be some limitations in evaluating the expression of AQP4, which shows a polarized pattern in the astrocyte end-feet. Through 3D culture, the expression of AQP4 in the astrocyte end-feet can be determined more accurately. The 3D-perfused system provides physiologically relevant insight and is more beneficial for evaluating the underlying signaling mechanisms and functions. In this regard, future studies need to utilize real-time monitoring of AQP4 expression using a 3D-self-organized model or a microvessel-on-a-chip platform [64, 65].

Importantly, we found that the treatment of mice with intracerebral hemorrhage with ROS scavenger significantly reduced PHE volume, which is likely via the restoration of the water channel AQP4 that promotes the clearance of excessive water buildup. Conversely, the experiments using AQP4$^{-/-}$ mice and an AQP4 enhancer suggested that AQP4 also has a pivotal role in suppressing the PHE formation by maintaining BBB's structural integrity. Thus, our results collectively suggest that AQP4 may be a useful clinical target for treating the PHE and its prevention. Although some potential AQP modulators have been identified, there are challenges associated with developing better modulators such as the druggability of the target and the suitability of the assay methods used for identifying potential modulators. Therefore, various advanced attempts are needed to develop new drugs targeting AQPs. In addition, screening of extensive libraries with efficient high-throughput screening (HTS) has become a vital process in drug discovery. HTS can screen thousands of compounds per day; however, if fewer compounds could be screened without compromising the probability of success, the cost and time would be largely reduced. Finally, recent advances in computer-aided design, in silico libraries, and molecular docking software combined with the upscaling of cell-based platforms have evolved to improve screening efficiency with higher predictability and clinical applicability [60, 66, 67].

Supplementary Information The online version contains supplementary material available at https://doi.org/10.1007/s13311-021-01126-2.

Acknowledgements We thank Junghui Lee for providing the clinical data and Soyoung Jung for summarizing the clinical cases. We are also grateful to Dr. Chong Jai Kim for his generous support in equipment and clinical resources. We thank the Magnetic Resonance Core facilities, the Confocal Microscope Core, and the Laboratory of Animal Research at the ConveRgencemEDIcine research center (CREDIT) at Asan Medical Center for their equipment, services, and expertise. Selective Plane Illumination Microscopy Light-sheet Z.1 was supported by the Brain Research Core Facilities at KBRI.

Required Author Forms Disclosure forms provided by the authors are available with the online version of this article.

Disclosures The authors declare no competing interests.

Funding This research was supported by a grant of the Korea Health Technology R&D Project through the Korea Health Industry Development Institute (KHIDI), funded by the Ministry of Health & Welfare, Republic of Korea (grant number: HI18C2383). The Basic Science Research Program supported this research through the National Research Foundation of Korea (NRF) funded by the Ministry of Education (2017R1D1A1B04035927), and 2019IL0828, 2019IP0779, and 2020IP0001 from the Asan Institute for Life sciences, Asan Medical Center (Seoul, Republic of Korea).

References

1. Qureshi, A.I., A.D. Mendelow, and D.F. Hanley, *Intracerebral haemorrhage.* Lancet, 2009. **373**(9675): p. 1632-44.
2. Qureshi, A.I., et al., *Spontaneous intracerebral hemorrhage.* N Engl J Med, 2001. **344**(19): p. 1450-60.
3. Stokum, J.A., V. Gerzanich, and J.M. Simard, *Molecular pathophysiology of cerebral edema.* J Cereb Blood Flow Metab, 2016. **36**(3): p. 513-38.
4. Simard, J.M., et al., *Brain oedema in focal ischaemia: molecular pathophysiology and theoretical implications.* Lancet Neurol, 2007. **6**(3): p. 258-68.
5. Armulik, A., et al., *Pericytes regulate the blood-brain barrier.* Nature, 2010. **468**(7323): p. 557-61.
6. Bell, R.D., et al., *Pericytes control key neurovascular functions and neuronal phenotype in the adult brain and during brain aging.* Neuron, 2010. **68**(3): p. 409-27.
7. King, L.S., D. Kozono, and P. Agre, *From structure to disease: the evolving tale of aquaporin biology.* Nat Rev Mol Cell Biol, 2004. **5**(9): p. 687-98.
8. Day, R.E., et al., *Human aquaporins: regulators of transcellular water flow.* Biochim Biophys Acta, 2014. **1840**(5): p. 1492-506.
9. Haj-Yasein, N.N., et al., *Glial-conditional deletion of aquaporin-4 (Aqp4) reduces blood-brain water uptake and confers barrier function on perivascular astrocyte endfeet.* Proc Natl Acad Sci U S A, 2011. **108**(43): p. 17815-20.

10. Hara-Chikuma, M. and A.S. Verkman, *Physiological roles of glycerol-transporting aquaporins: the aquaglyceroporins.* Cell Mol Life Sci, 2006. **63**(12): p. 1386-92.
11. Kitchen, P., et al., *Beyond water homeostasis: Diverse functional roles of mammalian aquaporins.* Biochim Biophys Acta, 2015. **1850**(12): p. 2410-21.
12. Kitchen, P., et al., *Water channel pore size determines exclusion properties but not solute selectivity.* Sci Rep, 2019. **9**(1): p. 20369.
13. Tomassoni, D., V. Bramanti, and F. Amenta, *Expression of aquaporins 1 and 4 in the brain of spontaneously hypertensive rats.* Brain Res, 2010. **1325**: p. 155-63.
14. Xi, T., et al., *miR-27a-3p protects against blood-brain barrier disruption and brain injury after intracerebral hemorrhage by targeting endothelial aquaporin-11.* J Biol Chem, 2018. **293**(52): p. 20041-20050.
15. Papadopoulos, M.C. and A.S. Verkman, *Aquaporin water channels in the nervous system.* Nat Rev Neurosci, 2013. **14**(4): p. 265-77.
16. Tait, M.J., et al., *Water movements in the brain: role of aquaporins.* Trends Neurosci, 2008. **31**(1): p. 37-43.
17. Papadopoulos, M.C., et al., *Aquaporin-4 facilitates reabsorption of excess fluid in vasogenic brain edema.* Faseb j, 2004. **18**(11): p. 1291-3.
18. Thrane, A.S., et al., *Critical role of aquaporin-4 (AQP4) in astrocytic Ca2+ signaling events elicited by cerebral edema.* Proc Natl Acad Sci U S A, 2011. **108**(2): p. 846-51.
19. Yang, B., Z. Zador, and A.S. Verkman, *Glial cell aquaporin-4 overexpression in transgenic mice accelerates cytotoxic brain swelling.* J Biol Chem, 2008. **283**(22): p. 15280-6.
20. Kitchen, P., et al., *Targeting Aquaporin-4 Subcellular Localization to Treat Central Nervous System Edema.* Cell, 2020. **181**(4): p. 784-799.e19.
21. Sylvain, N.J., et al., *The effects of trifluoperazine on brain edema, aquaporin-4 expression and metabolic markers during the acute phase of stroke using photothrombotic mouse model.* Biochim Biophys Acta Biomembr, 2021. **1863**(5): p. 183573.
22. Rynkowski, M.A., et al., *A mouse model of intracerebral hemorrhage using autologous blood infusion.* Nat Protoc, 2008. **3**(1): p. 122-8.
23. Parry-Jones, A.R., et al., *Edema Extension Distance: Outcome Measure for Phase II Clinical Trials Targeting Edema After Intracerebral Hemorrhage.* Stroke, 2015. **46**(6): p. e137-40.
24. Parry-Jones, A.R., et al., *Edema Extension Distance.* Stroke, 2015. **46**(6): p. e137-e140.
25. Wu, T.Y., et al., *Natural History of Perihematomal Edema and Impact on Outcome After Intracerebral Hemorrhage.* Stroke, 2017. **48**(4): p. 873-879.
26. Karuppagounder, S.S., et al., *N-acetylcysteine targets 5 lipoxygenase-derived, toxic lipids and can synergize with prostaglandin E(2) to inhibit ferroptosis and improve outcomes following hemorrhagic stroke in mice.* Ann Neurol, 2018. **84**(6): p. 854-872.
27. Zille, M., et al., *Neuronal Death After Hemorrhagic Stroke In Vitro and In Vivo Shares Features of Ferroptosis and Necroptosis.* Stroke, 2017. **48**(4): p. 1033-1043.
28. Moldes, O., et al., *Neuroprotection afforded by antagonists of endothelin-1 receptors in experimental stroke.* Neuropharmacology, 2012. **63**(8): p. 1279-85.
29. Li, J., et al., *TGN-020 alleviates edema and inhibits astrocyte activation and glial scar formation after spinal cord compression injury in rats.* Life Sci, 2019. **222**: p. 148-157.
30. Helms, H.C., et al., *In vitro models of the blood-brain barrier: An overview of commonly used brain endothelial cell culture models and guidelines for their use.* J Cereb Blood Flow Metab, 2016. **36**(5): p. 862-90.
31. Kim, J.E., H.J. Ryu, and T.C. Kang, *Status epilepticus induces vasogenic edema via tumor necrosis factor-α/ endothelin-1-mediated two different pathways.* PLoS One, 2013. **8**(9): p. e74458.
32. Balami, J.S. and A.M. Buchan, *Complications of intracerebral haemorrhage.* Lancet Neurol, 2012. **11**(1): p. 101-18.
33. Urday, S., et al., *Targeting secondary injury in intracerebral haemorrhage--perihaematomal oedema.* Nat Rev Neurol, 2015. **11**(2): p. 111-22.
34. Dienel, G.A., *Brain lactate metabolism: the discoveries and the controversies.* J Cereb Blood Flow Metab, 2012. **32**(7): p. 1107-38.
35. Ebert, D., R.G. Haller, and M.E. Walton, *Energy contribution of octanoate to intact rat brain metabolism measured by 13C nuclear magnetic resonance spectroscopy.* J Neurosci, 2003. **23**(13): p. 5928-35.
36. Hasselbalch, S.G., et al., *Brain Metabolism during Short-Term Starvation in Humans.* Journal of Cerebral Blood Flow & Metabolism, 1994. **14**(1): p. 125-131.
37. Owen, O.E., et al., *Brain metabolism during fasting.* The Journal of clinical investigation, 1967. **46**(10): p. 1589-1595.
38. Pellerin, L. and P.J. Magistretti, *Glutamate uptake into astrocytes stimulates aerobic glycolysis: a mechanism coupling neuronal activity to glucose utilization.* Proc Natl Acad Sci U S A, 1994. **91**(22): p. 10625-9.
39. Bak, L.K., et al., *Neuronal glucose but not lactate utilization is positively correlated with NMDA-induced neurotransmission and fluctuations in cytosolic Ca2+ levels.* J Neurochem, 2009. **109 Suppl 1**: p. 87-93.
40. Bordone, M.P., et al., *The energetic brain - A review from students to students.* J Neurochem, 2019. **151**(2): p. 139-165.
41. Mestre, H., et al., *Aquaporin-4-dependent glymphatic solute transport in the rodent brain.* Elife, 2018. **7**.
42. Zador, Z., et al., *Role of aquaporin-4 in cerebral edema and stroke.* Handb Exp Pharmacol, 2009(190): p. 159-70.
43. Dziedzic, T., et al., *Intracerebral hemorrhage triggers interleukin-6 and interleukin-10 release in blood.* Stroke, 2002. **33**(9): p. 2334-5.
44. Gurney, K.J., E.Y. Estrada, and G.A. Rosenberg, *Blood-brain barrier disruption by stromelysin-1 facilitates neutrophil infiltration in neuroinflammation.* Neurobiol Dis, 2006. **23**(1): p. 87-96.
45. de Oliveira Manoel, A.L., et al., *The critical care management of poor-grade subarachnoid haemorrhage.* Crit Care, 2016. **20**: p. 21.
46. Hu, X., et al., *Cerebral Vascular Disease and Neurovascular Injury in Ischemic Stroke.* Circ Res, 2017. **120**(3): p. 449-471.
47. Suzuki, Y., N. Nagai, and K. Umemura, *A Review of the Mechanisms of Blood-Brain Barrier Permeability by Tissue-Type Plasminogen Activator Treatment for Cerebral Ischemia.* Frontiers in cellular neuroscience, 2016. **10**: p. 2-2.
48. Bardehle, S., V.A. Rafalski, and K. Akassoglou, *Breaking boundaries-coagulation and fibrinolysis at the neurovascular interface.* Front Cell Neurosci, 2015. **9**: p. 354.
49. Rohde, V., et al., *Fibrinolysis therapy achieved with tissue plasminogen activator and aspiration of the liquefied clot after experimental intracerebral hemorrhage: rapid reduction in hematoma volume but intensification of delayed edema formation.* J Neurosurg, 2002. **97**(4): p. 954-62.
50. Turner, R.J. and F.R. Sharp, *Implications of MMP9 for Blood Brain Barrier Disruption and Hemorrhagic Transformation Following Ischemic Stroke.* Frontiers in cellular neuroscience, 2016. **10**: p. 56-56.
51. Ma, Y., et al., *The biphasic function of microglia in ischemic stroke.* Prog Neurobiol, 2017. **157**: p. 247-272.
52. Duan, X., et al., *Intracerebral Hemorrhage, Oxidative Stress, and Antioxidant Therapy.* Oxidative medicine and cellular longevity, 2016. **2016**: p. 1203285-1203285.
53. Qu, J., et al., *The Injury and Therapy of Reactive Oxygen Species in Intracerebral Hemorrhage Looking at Mitochondria.* Oxidative medicine and cellular longevity, 2016. **2016**: p. 2592935-2592935.
54. Ciappelloni, S., et al., *Aquaporin-4 Surface Trafficking Regulates Astrocytic Process Motility and Synaptic Activity in Health and Autoimmune Disease.* Cell Rep, 2019. **27**(13): p. 3860-3872.e4.

55. Salman, M.M., et al., *Hypothermia increases aquaporin 4 (AQP4) plasma membrane abundance in human primary cortical astrocytes via a calcium/transient receptor potential vanilloid 4 (TRPV4)- and calmodulin-mediated mechanism.* The European journal of neuroscience, 2017. **46**(9): p. 2542-2547.
56. Naval, N.S., et al., *An association of prior statin use with decreased perihematomal edema.* Neurocrit Care, 2008. **8**(1): p. 13-8.
57. Chen, Y., et al., *Endothelial NO synthase and reactive oxygen species mediated effect of simvastatin on vessel structure and function: pleiotropic and dose-dependent effect on tumor vascular stabilization.* Int J Oncol, 2013. **42**(4): p. 1325-36.
58. Witsch, J., et al., *Statins and perihemorrhagic edema in patients with spontaneous intracerebral hemorrhage.* Neurology, 2019. **92**(18): p. e2145-e2149.
59. Simard, J.M., et al., *Does inhibiting Sur1 complement rt-PA in cerebral ischemia?* Annals of the New York Academy of Sciences, 2012. **1268**: p. 95-107.
60. Verkman, A.S., M.O. Anderson, and M.C. Papadopoulos, *Aquaporins: important but elusive drug targets.* Nat Rev Drug Discov, 2014. **13**(4): p. 259-77.
61. Abir-Awan, M., et al., *Inhibitors of Mammalian Aquaporin Water Channels.* International journal of molecular sciences, 2019. **20**(7): p. 1589.
62. Kitchen, P., et al., *Identification and Molecular Mechanisms of the Rapid Tonicity-induced Relocalization of the Aquaporin 4 Channel.* J Biol Chem, 2015. **290**(27): p. 16873-81.
63. Verkman, A.S., et al., *The aquaporin-4 water channel as a potential drug target in neurological disorders.* Expert opinion on therapeutic targets, 2017. **21**(12): p. 1161-1170.
64. Salman, M.M., et al., *Design and Validation of a Human Brain Endothelial Microvessel-on-a-Chip Open Microfluidic Model Enabling Advanced Optical Imaging.* Front Bioeng Biotechnol, 2020. **8**: p. 573775.
65. Wevers, N.R., et al., *A perfused human blood-brain barrier on-a-chip for high-throughput assessment of barrier function and antibody transport.* Fluids Barriers CNS, 2018. **15**(1): p. 23.
66. Aldewachi, H., et al., *High-Throughput Screening Platforms in the Discovery of Novel Drugs for Neurodegenerative Diseases.* Bioengineering (Basel), 2021. **8**(2).
67. Salman, M.M., et al., *Advances in Applying Computer-Aided Drug Design for Neurodegenerative Diseases.* International Journal of Molecular Sciences, 2021. **22**(9): p. 4688.